Journal of Pharmacological Sciences 147 (2021) 156–167

Contents lists available at ScienceDirect

Journal of Pharmacological Sciences

journal homepage: www.elsevier.com/locate/jphs

Full Paper

3-Methyladenine prevents energy stress-induced necrotic death of melanoma cells through autophagy-independent mechanisms

Milica Kosic [a, 1], Verica Paunovic [a, 1], Biljana Ristic [a], Aleksandar Mircic [b], Mihajlo Bosnjak [b], Danijela Stevanovic [a], Tamara Kravic-Stevovic [b], Vladimir Trajkovic [a, **], Ljubica Harhaji-Trajkovic [c, *]

[a] Institute of Microbiology and Immunology, Faculty of Medicine, University of Belgrade, Dr. Subotica 1, 11000, Belgrade, Serbia
[b] Institute of Histology and Embryology, Faculty of Medicine, University of Belgrade, Visegradska 26, 11000, Belgrade, Serbia
[c] Department of Neurophysiology, Institute for Biological Research, "Sinisa Stankovic"- National Institute of Republic of Serbia, University of Belgrade, Despot Stefan Blvd. 142, 11000, Belgrade, Serbia

ARTICLE INFO

Article history:
Received 15 December 2020
Received in revised form
19 April 2021
Accepted 7 June 2021
Available online 11 June 2021

Keywords:
3-Methyladenine
Glycolysis
Mitochondria
Autophagy
Necrosis

ABSTRACT

We investigated the effect of 3-methyladenine (3MA), a class III phosphatidylinositol 3-kinase (PI3K)-blocking autophagy inhibitor, on cancer cell death induced by simultaneous inhibition of glycolysis by 2-deoxyglucose (2DG) and mitochondrial respiration by rotenone. 2DG/rotenone reduced ATP levels and increased mitochondrial superoxide production, causing mitochondrial swelling and necrotic death in various cancer cell lines. 2DG/rotenone failed to increase proautophagic beclin-1 and autophagic flux in melanoma cells despite the activation of AMP-activated protein kinase (AMPK) and inhibition of mechanistic target of rapamycin complex 1 (mTORC1). 3MA, but not autophagy inhibition with other PI3K and lysosomal inhibitors, attenuated 2DG/rotenone-induced mitochondrial damage, oxidative stress, ATP depletion, and cell death, while antioxidant treatment mimicked its protective action. The protection was not mediated by autophagy upregulation via class I PI3K/Akt inhibition, as it was preserved in cells with genetically inhibited autophagy. 3MA increased AMPK and mTORC1 activation in energy-stressed cells, but neither AMPK nor mTORC1 inhibition reduced its cytoprotective effect. 3MA reduced JNK activation, and JNK pharmacological/genetic suppression mimicked its mitochondria-preserving and cytoprotective activity. Therefore, 3MA prevents energy stress-triggered cancer cell death through autophagy-independent mechanisms possibly involving JNK suppression and decrease of oxidative stress. Our results warrant caution when using 3MA as an autophagy inhibitor.

1. Introduction

Macroautophagy (hereafter autophagy) is a process in which intracellular proteins and organelles are sequestered within double-membrane autophagosomes, which deliver their cargo to lysosomes for degradation and recycling.[1] Autophagy proceeds through the coordinated engagement of autophagy-related (ATG) proteins involved in initiation and autophagosome formation, maturation, and fusion with lysosome. The main autophagy-initiating signaling pathway is energy stress-mediated activation of the intracellular energy sensor AMP-activated protein kinase (AMPK), followed by the inhibition of the mechanistic target of rapamycin complex 1 (mTORC1), the principal suppressor of autophagy.[1] Conversely, stimulation of Akt by various growth factors leads to mTORC1 activation and autophagy suppression.[1] By removing damaged organelles, protein aggregates, as well as by providing new building blocks and energy for cellular homeostasis, autophagy plays an important role in the adaptive protective response against metabolic, hypoxic, oxidative, proteotoxic, and drug-induced stress.[1] However, in certain conditions autophagy can contribute to apoptotic/necrotic cell demise or function as an

* Corresponding author. Fax: +381113643235.
** Corresponding author. Fax: +381113643235.
E-mail addresses: vladimir.trajkovic@med.bg.ac.rs (V. Trajkovic), buajk@yahoo.com (L. Harhaji-Trajkovic).
Peer review under responsibility of Japanese Pharmacological Society.
[1] Equally contributing authors.

https://doi.org/10.1016/j.jphs.2021.06.003

alternative programmed cell-death pathway.[2] Deficient or overactive autophagy is associated with the pathogenesis and progression of multiple disorders, including malignant, metabolic, neurodegenerative, cardiovascular, and autoimmune/inflammatory diseases.[2] The rationale behind the current exploration of autophagy inhibitors in cancer therapy is to counteract the protective action of autophagic response triggered by energy stress in cancer cells exposed to nutrient/oxygen deprivation and/or chemotherapy.[3] Autophagy signaling, autophagosome formation/maturation, and lysosomal degradation are all potentially druggable processes, and the selectivity of autophagy modulators has to be carefully considered in various experimental and therapeutic settings.

3-methyladenine (3MA), together with wortmannin and LY294002, belongs to a group of phosphatidylinositol 3-kinase (PI3K) inhibitors that block autophagy at the initiation and maturation stages by preventing the class III PI3K interaction with various ATG partners.[4] While mainly used for autophagy research *in vitro*, the potential therapeutic usefulness of 3MA-mediated autophagy inhibition has been indicated by its beneficial effects in animal models of cancer.[5–7] However, prolonged exposure to 3MA, but not other class III PI3K inhibitors, can promote autophagy in nutrient-rich conditions through persistent inactivation of class I PI3K and subsequent inhibition of Akt/mTORC1 pathway.[8,9] Moreover, 3MA can affect other kinases and cellular processes such as glycogen metabolism, endocytosis, proteolysis, and mitochondrial permeability transition in an autophagy-independent manner.[10–13] Despite these, cytoprotective effects of 3MA in various experimental settings have been frequently ascribed to autophagy suppression, without directly confirming (e.g. by genetic approaches) the role of autophagy in the observed cell death.[14–16] It is also worth noting that 3MA is excised by 3MA DNA glycosylase from DNA alkylated spontaneously or by environmental toxins and chemotherapeutic agents,[17] causing its levels to increase in the urine of cancer patients receiving chemotherapy.[18] However, while unrepaired 3MA is a potentially lethal lesion in cancer cells,[19] the biological roles of the excised 3MA are not known.

In the present study, we explored the potential of various autophagy inhibitors, including 3MA, to affect energy stress-triggered death of cancer cells exposed to simultaneous blockade of glycolysis and mitochondrial respiration, both used by tumor cells to sustain their high energy demands. Surprisingly, while neither of autophagy blockers was able to increase energy stress-induced cell death, 3MA promoted their survival through autophagy-independent mechanisms possibly involving the inhibition of oxidative stress and c-Jun N-terminal kinase (JNK).

2. Material and methods

2.1. Cell culture

Mouse melanoma B16, mouse fibrosarcoma L929, and human glioblastoma U251 cell lines purchased from the European Collection of Animal Cell Cultures (Salisbury, UK) were maintained and plated for experiments exactly as previously described.[20] Primary mouse (C57BL/6) mesenchymal stem cells (Invitrogen, Paisley, UK; S1502-100) were kindly provided by Dr. Vladislav Volarevic (Faculty of Medical Sciences, University of Kragujevac, Serbia). Cells were maintained at 37 °C in a humidified atmosphere with 5% CO_2 and 20% O_2 (or 1% O_2 for hypoxia evaluation), in a HEPES-buffered RPMI 1640 cell culture medium with L-glutamine, supplemented with 10% fetal bovine serum (FBS) for B16 and MSC cells and 5% FBS for U251 and L929 cells, 1 mM sodium pyruvate and antibiotic/antimycotic (all purchased from GE Healthcare, Chicago, Illinois). After resting for 24 h cells were treated with glycolysis inhibitor 2-deoxyglucose (2DG) and/or mitochondrial complex I inhibitor rotenone, in the presence or absence of antioxidant α-tocopherol, mitochondrial permeability transition (MPT) inhibitor cyclosporine A, glycolysis inhibitor iodoacetate, oxidative phosphorylation inhibitors carbonyl cyanide m-chlorophenyl hydrazone (CCCP) and 1-methyl-4-phenylpyridinium (MPP+), autophagy inhibitors 3MA, bafilomycin A1, chloroquine, and ammonium chloride, mTORC1 inhibitor rapamycin, caspase inhibitors Z-VAD-FMK and Q-VD-OPh, necroptosis inhibitor necrostatin-1, PI3K inhibitors wortmannin or LY29400, Akt inhibitor 10-(4'-(N-diethylamino)butyl)-2-chlorophenoxazine (DEBC), extracellular signal kinase (ERK) inhibitor PD098059, JNK inhibitor SP600125, adenylyl cyclase activator forskolin, or cAMP analogue 8-Chloro-cAMP (8-Cl-cAMP) (all from Merck, Darmstadt, Germany). The cytotoxic drug cisplatin (Merck, Darmstadt, Germany) was used in some experiments as a positive control.

2.2. Phase contrast and transmission electron microscopy (TEM)

Cell morphology was determined using a phase contrast microscope (Leica Microsystems DMIL, Wetzlar, Germany) equipped with Leica Microsystems DFC320 camera and Leica Application Suite software (version 2.8.1). For the ultrastructural analysis by TEM, trypsinized cells were fixed in 3% glutaraldehyde, postfixed in 1% osmium tetroxide, dehydrated in graded alcohols and then embedded in Epon 812 (all from Merck, Darmstadt, Germany). The ultrathin sections were stained in uranyl acetate and lead citrate and examined using a Morgagni 268D electron microscope (FEI, Hillsboro, OR).

2.3. Lactate dehydrogenase (LDH) cytotoxicity assay

The release of the intracellular enzyme LDH, as a marker of cell membrane damage, was used to determine cytotoxicity of various treatments. Briefly, 50 μl of cell culture supernatant was mixed with 50 μl of solution containing 54 mM lactic acid, 0.28 mM phenazine methosulfate, 0.66 mM p-iodonitrotetrazolium chloride and 1.3 mM βNAD. The pyruvate-mediated conversion of 2,4-dinitrophenylhydrazine into visible hydrazone precipitate was measured using an automated microplate reader at 492 nm. The percentage of dead cells was determined using the following formula: $[(E-C)/(T-C)]\times 100$, where E is the experimental absorbance of treated cells, C is the control absorbance of medium without cells, and T is the absorbance corresponding to the maximal (100%) LDH release of Triton X-100-lysed cells.

2.4. Apoptosis/necrosis and caspase activation analysis

Apoptotic and necrotic cell death were analyzed by flow cytometry following double staining with annexin V-fluorescein isothiocyanate (FITC) and 7-aminoactinomycin D (7AAD), in which annexin V binds to cells with exposed phosphatidylserine, while 7AAD labels the cells with membrane damage. Staining was performed according to the instructions by the manufacturer (BD Biosciences, San Diego, CA), and the percentages of viable (annexin$^-$/7AAD$^-$), apoptotic (annexin$^+$/7AAD$^-$), and necrotic (annexin$^+$/7AAD$^+$) cells were determined using flow cytometry. DNA fragmentation, as a feature of apoptotic cell death, was determined by cell cycle analysis. Briefly, the cells were fixed in 70% ethanol at 4 °C for 30 min. Before analysis, ethanol was removed by centrifugation and cells were washed twice with PBS. Cells were then resuspended in PBS containing 1 mg/ml RNase and propidium iodide (40 μg/ml) (both from Merck, Darmstadt, Germany) and kept at 37 °C in the dark for 30 min. The proportion of apoptotic cells

with fragmented DNA in the subG$_0$/G$_1$ compartment of the cell cycle was determined by flow cytometry. Activation of caspases was measured using a cell-permeable, FITC-conjugated pan-caspase inhibitor Z-VAD-FMK (ApoStat; R&D Systems, Minneapolis, MN) according to the manufacturer's instructions. The increase in green fluorescence as a measure of caspase activity was determined using flow cytometry and presented as the fold change in fluorescence intensity, which was arbitrarily set to 1 in untreated cells. All flow cytometric acquisitions were done on FACS Aria III flow cytometer using FACSDiva 6.0 software (BD Biosciences, San Diego, CA) and subsequently analyzed with FlowJo software (BD Biosciences, San Diego, CA).

2.5. Mitochondrial membrane potential and superoxide measurement

Mitochondrial membrane potential was measured using JC-1 (Trevigen Inc., Gaithersburg, MD), a lipophilic cation that aggregates upon mitochondrial membrane polarization thus forming an orange-red fluorescent compound. When the membrane potential is disrupted, the dye cannot access the transmembrane space and remains or reverts to its green monomeric form. The cells were stained with JC-1 dye as described by the manufacturer, and the fluorescence emitted by the green monomers and red aggregates was detected by flow cytometry. The increase and decrease in green/red fluorescence ratio reflect mitochondrial membrane depolarization and hyperpolarization, respectively. The results are presented as a fold change of green/red fluorescence ratio in treated compared to the control cells. The production of mitochondria-derived superoxide was determined by measuring the intensity of red fluorescence emitted by a redox-sensitive dye MitoSOX Red (Thermo Fisher Scientific, Waltham, MA), according to the manufacturer's instructions. The mean intensity of MitoSOX Red fluorescence, corresponding to superoxide levels, was determined using flow cytometry and presented as the fold change in fluorescence intensity, which was arbitrarily set to 1 in untreated cells. Both JC-1 and MitoSOX measurements were done on FACS Aria III flow cytometer using FACSDiva 6.0 software for acquisition and FlowJo software for analysis.

2.6. Intracellular ATP quantification

The intracellular concentration of ATP was determined by Chameleon microplate reader (Hidex, Turku, Finland) using ATP Bioluminescence Assay Kit HS II (Roche Applied Science, Penzberg, Germany) according to the manufacturer's instructions. The results are presented as the fold change in luminescence intensity, which was arbitrarily set to 1 in untreated cells.

2.7. Immunoblotting

Cells were lysed in the lysis buffer (30 mM Tris–HCl pH 8.0, 150 mM NaCl, 1% NP-40 and protease/phosphatase inhibitor cocktail; all from Merck, Darmstadt, Germany), stored on ice for 30 min, centrifuged at 14,000 g for 15 min at 4 °C, and the supernatants were collected. Equal protein amounts from each sample were separated by sodium dodecyl sulfate-polyacrylamide gel electrophoresis and transferred to nitrocellulose membranes (Bio-Rad, Hercules, CA). Rabbit anti-mouse antibodies against cleaved caspase-3 (#9664), cytochrome *c* (#4280), Poly (ADP-ribose) polymerase (PARP; #9542), AMPKα (#2603), phospho-AMPKα (Thr172; #2535), microtubule-associated protein 1 light chain 3B (LC3B; #2775), mTOR (#2983), phospho-mTOR (Ser2448; #2971), eukaryotic translation initiation factor 4E-binding protein 1 (4EBP1; #9644), phospho-4EBP1 (Thr37/46; #2855), Akt (#9272), phospho-Akt (Ser473; #9271), JNK (#9252), phospho-JNK (Thr183/Tyr185; #9251), ERK (#9102), phospho-ERK (Thr202/Tyr204; #9101), actin (#4967) (all from Cell Signaling Technology, Beverly, MA), TOM20 (sc-11415) (Santa Cruz Biotechnology, Santa Cruz, CA), and beclin-1 (NB500-249; Novus Biologicals, Littleton, CO) were used as primary antibodies. Peroxidase-conjugated goat anti-rabbit IgG (#7074, Cell Signaling Technology, Beverly, MA) was used as a secondary antibody, and specific protein bands were visualized by enhanced chemiluminescence using ChemiDoc MP Imaging System (Bio-Rad, Hercules, CA). The intensity of protein bands was measured by densitometry using Image Lab software (Bio-Rad, Hercules, CA).

2.8. RNA interference (RNAi)

The transfection of cells with control small interfering RNA (siRNA) or siRNA against beclin-1, LC3, AMPK, or JNK (all from Santa Cruz Biotechnology, Dallas, TX) was performed using the SF Cell Line 4D-Nucleofector V Kit and 4D-Nucleofector (Lonza, Basel, Switzerland), according to the manufacturer's instructions. After transfection, cells were rested for 24 h before being used in experiments.

2.9. Statistical analysis

Statistical significance of the differences between treatments was assessed using t-test or one-way ANOVA followed by Tukey's test for multiple comparisons. A value of $p < 0.05$ was considered statistically significant.

3. Results

3.1. Simultaneous inhibition of glycolysis and mitochondrial respiration causes necrosis of cancer cells

To establish the optimal conditions for the induction of cell death through energy depletion, we treated B16 melanoma cells for 24 h with different doses of glycolysis inhibitor 2DG and mitochondrial inhibitor rotenone, separately or in combination, and cell death was assessed by LDH release assay. While neither compound alone affected cell viability, the combined treatment increased LDH levels in the cell culture supernatants in a dose-dependent manner, thus reflecting the loss of cell membrane integrity (Fig. 1A). For further studies, we have chosen the combination of 5 mM 2DG and 1 μM rotenone. 2DG and rotenone at the chosen concentrations also synergized in inducing cell death of L929 fibrosarcoma and U251 glioma cells, but failed to do so in non-cancerous mesenchymal stem cells (Fig. 1B). B16 were selected for further experiments because of the slightly higher sensitivity (Fig. 1B). A similar cytotoxic effect was also obtained by using rotenone with glycolysis inhibitor iodoacetate or in a cell culture medium without glucose (Fig. 1C), as well as by combining 2DG with mitochondrial complex I inhibitor MPP+, mitochondrial uncoupler CCCP, or hypoxia (1% O_2) (Fig. 1D). These data confirmed that the synergistic cytotoxicity resulted from the simultaneous inhibition of glycolysis and mitochondrial respiration. Flow cytometric analysis of annexin-V/7AAD-stained cells revealed a synergistic induction of cell membrane damage by the two compounds, as shown by the time-dependent increase in the numbers of double-positive cells (Fig. 1E and F). The absence of truly apoptotic cells with externalized phosphatidylserine and no membrane damage ($Ann^+/7AAD^-$) at earlier time points (not shown) indicated the induction of primary, rather than secondary necrosis. Accordingly, the cell cycle analysis did not detect hypodiploid (sub-G) apoptotic cells with fragmented DNA upon 2DG/rotenone treatment (Fig. 1G), and

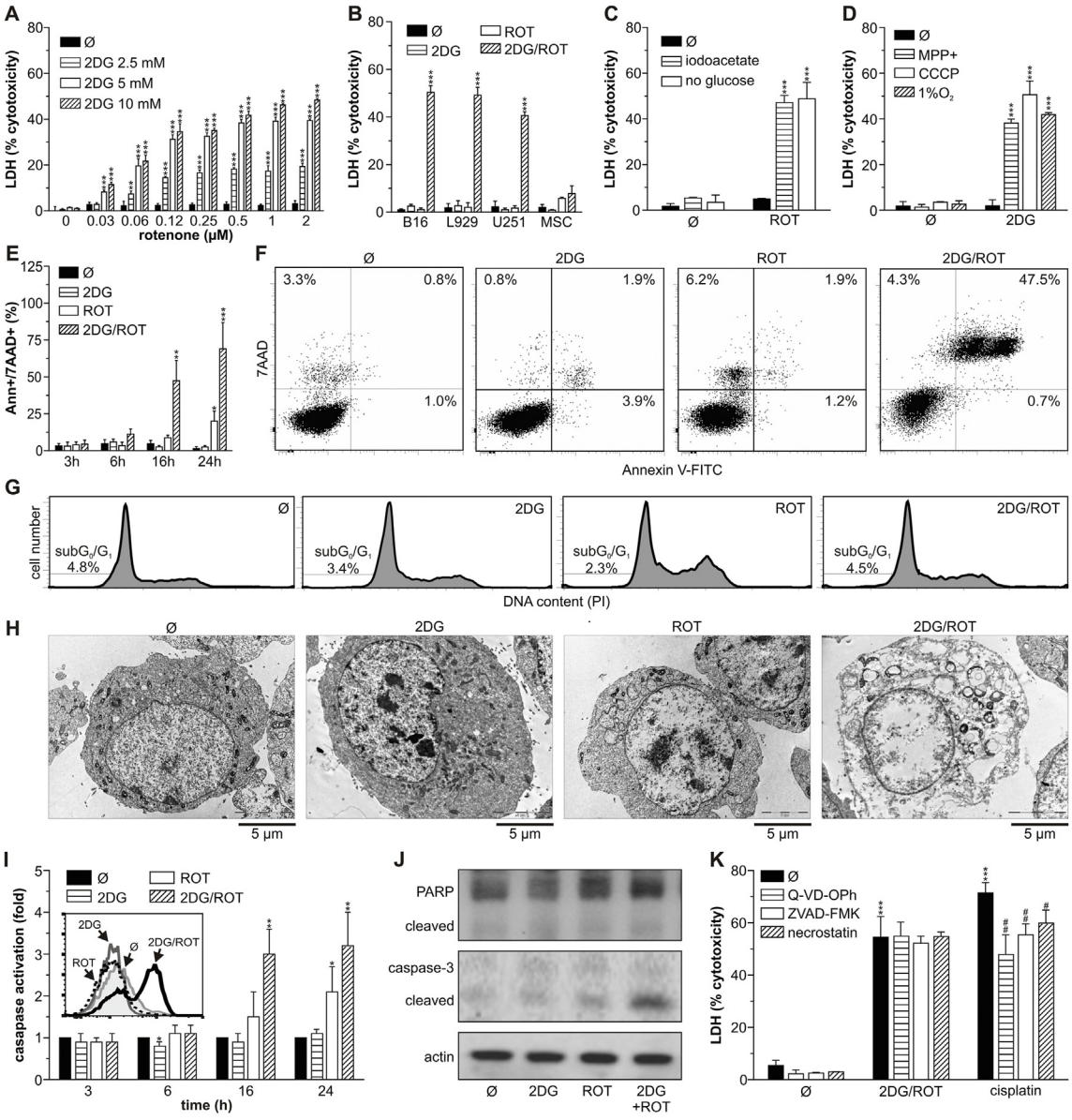

Fig. 1. Simultaneous inhibition of glycolysis and mitochondrial respiration causes necrotic cell death. (A) B16 cells were incubated with different doses of 2DG or rotenone (ROT) alone and in combination. (B) B16, L929, U251, and mesenchymal stem cells (MSC) were incubated with 2DG (5 mM) or rotenone (1 μM) alone and in combination. (C) B16 cells were incubated with rotenone (1 μM) in medium with or without glucose or glycolytic inhibitor iodoacetate (IA; 4 μM). (D) B16 cells were incubated with 2DG (5 mM) in the absence or presence of oxidative phosphorylation inhibitors MPP+ (4 mM) and CCCP (30 μM) or hypoxia (1% O_2). (E–J) B16 cells were incubated with 2DG (5 mM) or rotenone (1 μM) alone and in combination. (K) B16 cells were incubated with 2DG (5 mM) and rotenone (1 μM) or cisplatin (50 μM) in the absence or presence of Q-VD-OPh (10 μM), Z-VAD-FMK (1 μM), or necrostatin (10 μM). (A-D, K) Cytotoxicity was assessed by LDH release assay after 24 h of treatment. (E–I) Phosphatidylserine externalization (annexin$^+$ cells) and cell membrane damage (7AAD$^+$ cells) (E, F), DNA fragmentation (G), and caspase activation in ApoStat-stained cells (I) were assessed by flow cytometry, while cell morphology was determined by TEM (H) after the indicated time periods (E, I), 16 h (F), 24 h (G, H). (J) Caspase-3 activation and PARP cleavage after 12 h of treatment were examined by immunoblotting. Representative flow cytometry dot-plots (F) and histograms (G, I), as well as TEM micrographs (H) and immunoblot images (J) are shown. The data are presented as mean ± SD values of triplicates from a representative of at least three experiments (A-D, K) or mean ± SD values of three independent experiments (E, I) (*$p < 0.05$, **$p < 0.01$, and ***$p < 0.001$ vs. no treatment).

apoptotic cells were also not observed by electron microscopy (Fig. 1H). While showing no obvious alterations of cell morphology in cells exposed to 2DG or rotenone alone, TEM analysis confirmed the necrotic appearance of cells treated with their combination, which displayed membrane disintegration and electron-lucent cytoplasm (Fig. 1H). Despite the absence of apoptosis, flow cytometric analysis displayed a time-dependent increase in the activation of apoptosis-inducing enzymes caspases (Fig. 1I), and immunoblotting confirmed the activation (cleavage) of the apoptosis-executing caspase-3 in B16 cells treated with 2DG/rotenone (Fig. 1J). However, a DNA-repairing enzyme PARP, which responds to DNA breaks during apoptosis, was not activated (cleaved) in 2DG/rotenone-exposed cells (Fig. 1J). Moreover, neither the inhibitors of apoptosis Q-VD-OPh and Z-VAD-FMK, nor necrostatin, inhibitor of necroptosis (programmed necrosis), were able to reduce 2DG/rotenone-induced cell death despite significantly attenuating the cytotoxicity of cisplatin (Fig. 1K). Collectively, these results demonstrate that the cancer cell demise induced by simultaneous inhibition of glycolysis and oxidative phosphorylation is mediated by necrosis, but not apoptosis or necroptosis.

3.2. 2DG/rotenone treatment induces mitochondrial damage associated with ATP depletion and superoxide production

Ultrastructural analysis of B16 cells treated with 2DG or rotenone alone revealed the presence of mitochondrial edema, with the majority of mitochondria being swollen, displaying condensed matrix and edematous cristae (Fig. 2A, black arrows). On the other hand, combined treatment caused more severe mitochondrial damage, where in addition to the edematous mitochondria, degraded or disintegrated mitochondria were observed, showing loss of matrix density and fragmentation and loss of the inner membrane cristae (Fig. 2A, white arrows). We next investigated effects of 2DG/rotenone treatment on mitochondrial function in B16 cells. 2DG and to the lesser extent rotenone reduced intracellular ATP levels, while combined treatment caused further ATP loss in a time-dependent manner (Fig. 2B). Flow cytometric analysis of JC-1 green/red fluorescence ratio revealed that rotenone caused fast and sustained mitochondrial depolarization, in contrast to the increase in mitochondrial membrane potential in 2DG-treated cells (Fig. 2C and D). In 2DG/rotenone-exposed cells mitochondria were significantly less depolarized compared to rotenone treatment, except at the latest time point (24 h) (Fig. 2D). While neither agent alone increased mitochondrial superoxide levels, they synergized in a time-dependent manner to increase its production, as confirmed by flow cytometric analysis of MitoSOX-stained cells (Fig. 2E). Moreover, α-tocopherol, an antioxidant able to both scavenge superoxide and suppress its mitochondrial generation,[21] reduced the cytotoxicity of 2DG/rotenone combination (Fig. 2F). On the other hand, MPT inhibitor cyclosporine A failed to exert any protection (Fig. 2G). Therefore, 2DG/rotenone-induced mitochondrial damage and subsequent necrosis were apparently mediated by synergistic induction of ATP loss and mitochondrial superoxide, independently of mitochondrial depolarization and MPT induction.

3.3. 3MA protects cancer cells from inhibition of glycolysis and mitochondrial respiration

As energy depletion usually triggers the protective autophagic response, we next tested the ability of various autophagy inhibitors to potentiate cell death induced by the inhibition of both glycolysis and oxidative phosphorylation. Surprisingly, autophagy suppression with lysosomal inhibitors bafilomycin A1, chloroquine, and NH_4Cl did not affect 2DG/rotenone-induced death of B16, L929, and U251 cells, while the administration of PI3K class III and autophagy initiation inhibitor 3MA resulted in a significant dose-dependent cell protection (Fig. 3A–D). Similar results were obtained when rotenone was replaced with MPP+, CCCP, or hypoxia (1% O_2) (Fig. 3E–G), or when 2DG was replaced with iodoacetate or

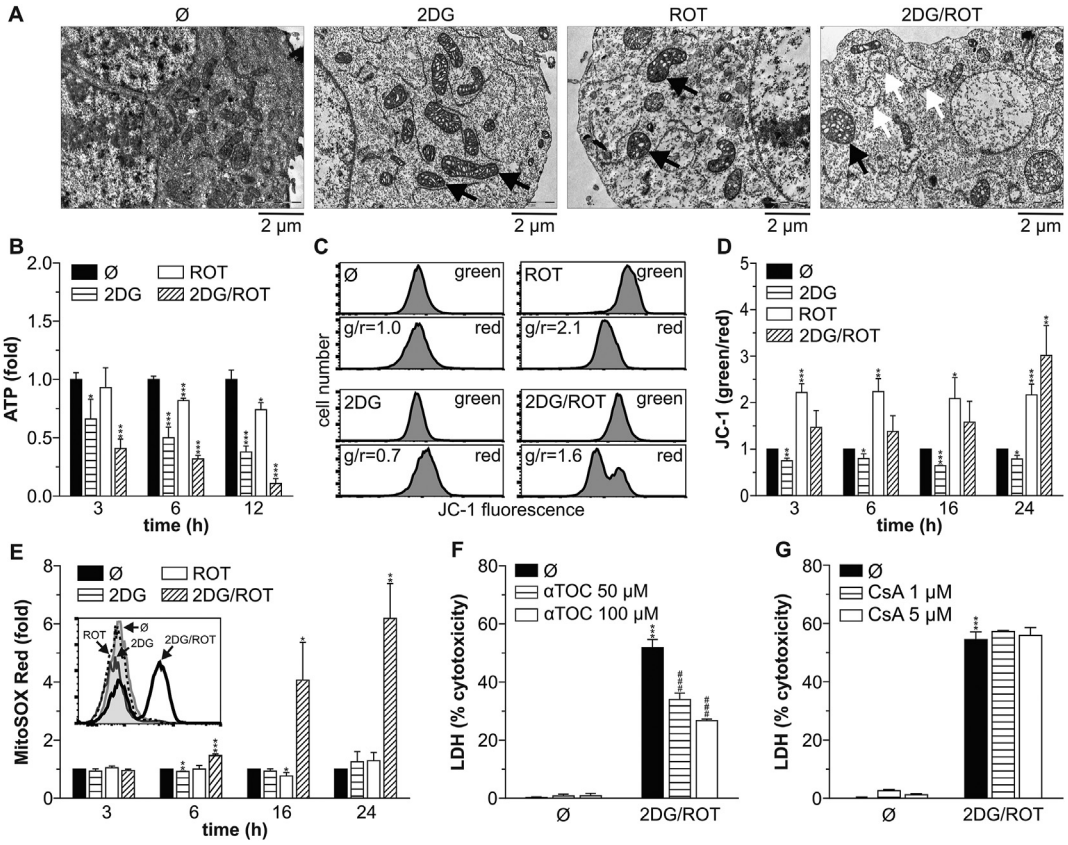

Fig. 2. 2DG/rotenone treatment induces mitochondrial damage associated with ATP depletion and superoxide production. (A–G) B16 cells were incubated with 2DG (5 mM) or rotenone (ROT; 1 μM) alone and in combination, in the presence or absence of α-tocopherol (αTOC) (F) or cyclosporine A (CsA) (G) for 24 h (A, F, G), 16 h (C), or the indicated time periods (B, D, E). Cell ultrastructural morphology was analyzed by TEM (A), intracellular ATP concentration was determined by bioluminescence assay (B), mitochondrial depolarization in JC-1-stained cells (C, D) and mitochondrial superoxide production in MitoSOX Red-stained cells (E) were measured by flow cytometry, and cytotoxicity was assessed by LDH release assay (F, G). The black and white arrows in (A) point to swollen but intact mitochondria and damaged mitochondria with fragmented cristae, respectively. The data are presented as mean ± SD values of triplicates from a representative of at least three experiments (B, F, G) or mean ± SD values of three independent experiments (D, E) (*$p < 0.05$, **$p < 0.01$, and ***$p < 0.001$ vs. no treatment; $^{###}p < 0.001$ vs. treatment with 2DG/rotenone).

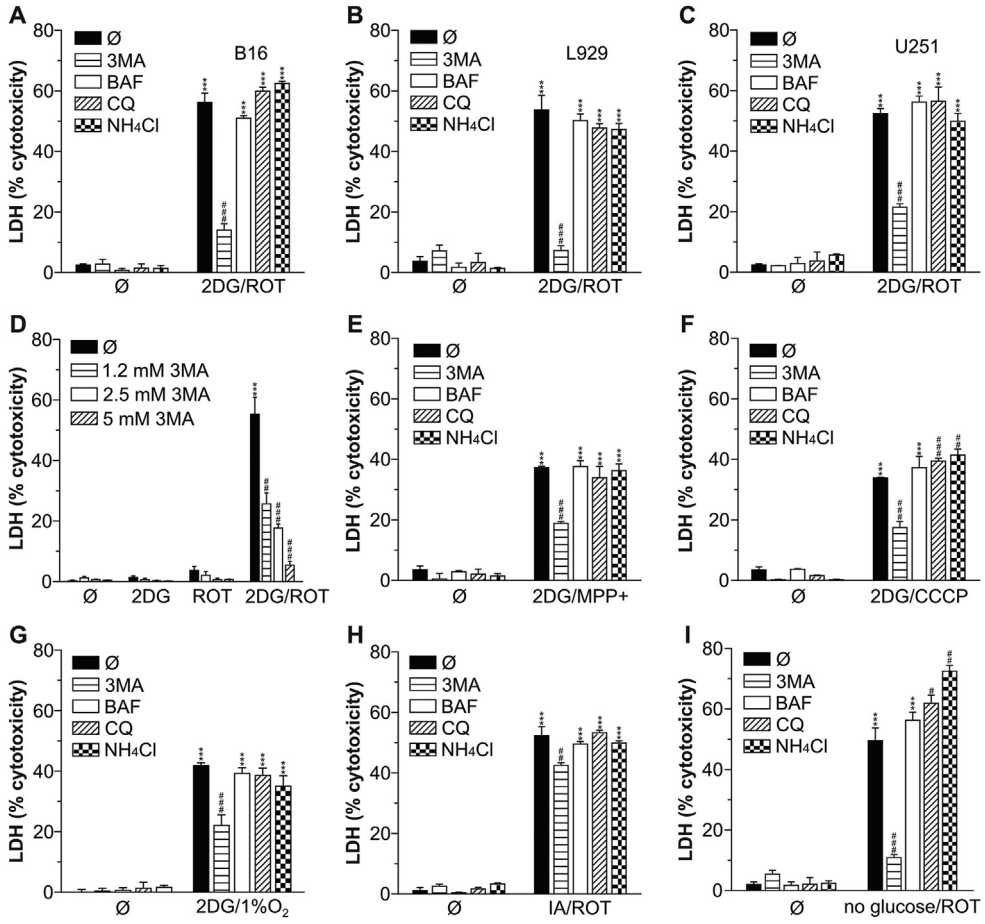

Fig. 3. 3MA protects cancer cells from inhibition of glycolysis and mitochondrial respiration. (A–I) B16 (A, D-I), L929 (B), or U251 cells (C) were treated for 24 h with the combination of 2DG (5 mM) and rotenone (ROT; 1 μM) (A–D), 2DG and MPP+ (4 mM) (E), CCCP (30 μM) (F), or hypoxia (1% O_2) (G), rotenone and iodoacetate (4 μM) (H) or glucose-free medium (I), in the absence or presence of autophagy inhibitors 3-methyladenine (3MA; 5 mM), bafilomycin A1 (BAF; 10 nM), chloroquine (CQ; 20 μM), or ammonium chloride (NH_4Cl; 10 mM). Cytotoxicity was determined by LDH release assay, and the data are presented as mean ± SD values of triplicates from a representative of at least three experiments (***$p < 0.001$ vs. no treatment; $^{\#\#}p < 0.01$ and $^{\#\#\#}p < 0.001$ vs. treatment with 2DG/rotenone (A–D), 2DG/MPP+ (E), 2DG/CCCP (F), 2DG/hypoxia (G), iodoacetate/rotenone (H), or glucose-free medium/rotenone (I)).

glucose-free medium (Fig. 3H–I), thus indicating that 3MA was indeed able to protect B16 cells from the simultaneous inhibition of glycolysis and mitochondrial respiration.

3.4. 3MA protects melanoma cells from 2DG/rotenone independently of autophagy

Next, we investigated the role of autophagy in the cytoprotective action of 3MA in B16 melanoma cells exposed to 2DG/rotenone. In agreement with previous results (Fig. 3A–C), RNAi silencing of autophagy-essential genes beclin-1 and LC3 failed to affect 2DG/rotenone cytotoxicity (Fig. 4A), indicating that the protective effect of 3MA was unrelated to autophagy inhibition. Moreover, the pro-survival effect of 3MA was completely preserved in beclin-1- and LC3-deficient cells (Fig. 4A), thus excluding the possibility that 3MA-mediated cytoprotection was due to previously described autophagy upregulation resulting from class I PI3K inhibition.[8] Somewhat unexpectedly, 2DG/rotenone decreased the conversion of LC3-I to its lipidated, autophagosome-associated form LC3-II (Fig. 4B), indicating suppression, rather than induction of autophagy. We also tested LC3-II accumulation in the presence of lysosomal inhibitor, as this approach, due to degradation of LC3-II by lysosomal hydrolases after formation of autolysosomes, reflects autophagic turnover (flux) better than the assessment of steady-state LC3-II levels.[22] Lysosomal degradation of LC3-II was inhibited by the V-ATPase proton pump blocker bafilomycin A1, which expectedly increased LC3-II accumulation (Fig. 4B). The additional treatment with 2DG/rotenone significantly reduced LC3-II levels compared to bafilomycin A1 alone (Fig. 4B), thus confirming the decrease in autophagic flux. Accordingly, 2DG/rotenone reduced the intracellular levels of autophagy activator beclin-1, with 3MA treatment causing no further change in beclin-1 expression (Fig. 4C). Moreover, 3MA had no significant effect on LC3 conversion in 2DG/rotenone treated cells (Fig. 4C). On the other hand, 3MA prevented LC3-II increase in cells treated with the well-known autophagy inducer cisplatin[23] (Fig. 4D) and increased its cytotoxicity similarly to other autophagy inhibitors (Fig. 4E). Together, these data demonstrate that 3MA protects cells from the simultaneous inhibition of glycolysis and oxidative phosphorylation independently of its autophagy-modulating effect and in a context-dependent manner.

3.5. 3MA-mediated protection from mitochondrial damage and necrosis is associated with decrease in superoxide production

We next explored the effects of 3MA on structural and functional integrity of mitochondria in 2DG/rotenone-treated B16 cells. The ability of 3MA to reduce necrotic morphology (Fig. 5A) and cell

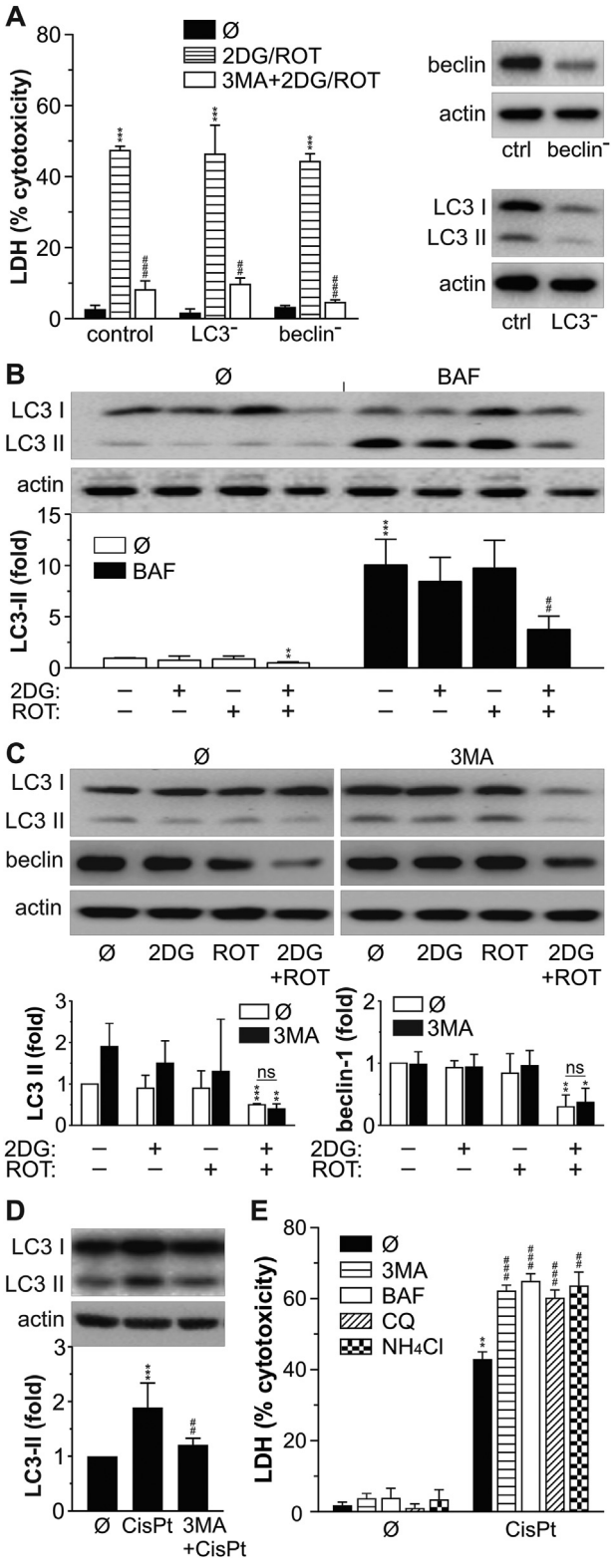

Fig. 4. 3MA protects melanoma cells from 2DG/rotenone independently of autophagy. (A) B16 cells transfected with control, beclin-1, or LC3B siRNA were incubated for 24 h with 2DG (5 mM) and rotenone (ROT, 1 μM) in the absence or presence of 3MA (5 mM) (immunoblots confirm the efficiency of beclin-1 and LC3B knockdown). (B, C) B16 cells were treated for 6 h with 2DG (5 mM) and ROT (1 μM), in the presence or absence of 10 nM bafilomycin A1 (B) or 5 mM 3MA (C). (D, E) B16 cells were treated with cisplatin (50 μM) in the presence or absence of 3MA (5 mM) for 6 h (D) or 3MA (5 mM), bafilomycin A1 (BAF; 10 nM), chloroquine (CQ; 20 μM), and ammonium chloride (NH_4Cl; 10 mM) for 24 h (E). Cytotoxicity was determined by LDH release assay (A, E).

membrane permeability to 7AAD in 2DG/rotenone-exposed cells (Fig. 5B) was associated with the increase in ATP synthesis (Fig. 5C) and decrease in mitochondrial superoxide production (Fig. 5D), indicating a partial recovery of mitochondrial function. While mitochondrial structure was not altered after treatment with 3MA alone, 2DG/rotenone combination, in accordance with the findings reported in Fig. 2A, caused severe mitochondrial damage with fragmentation of cristae and washed-out appearance of mitochondrial matrix (Fig. 5E, white arrows). On the other hand, mitochondria in 2DG/rotenone-exposed cells treated with 3MA displayed an improved morphology with preserved cristae, which was associated with the increased presence of donut-shaped mitochondria (Fig. 5E, black arrows). The donut shape of mitochondria has been associated with the mild levels of mitochondrial ROS and their ability to recover "healthy", low ROS-producing tubular shape.[24] Mitochondrial swelling causes the rupture of outer mitochondrial membrane, cytochrome *c* release from the intermembrane space, and subsequent activation of caspases.[25] Accordingly, 3MA prevented 2DG/rotenone-triggered caspase activation (Fig. 5F) and decrease in the mitochondrial content of cytochrome *c* (Fig. 5H). The observed effects of 3MA were not associated with the changes in mitochondrial membrane potential in 2DG/rotenone-treated cells (Fig. 5G). These data indicate that 3MA might prevent 2DG/rotenone-triggered mitochondrial damage and necrosis through mitochondrial membrane potential-independent decrease in superoxide generation.

3.6. Cytoprotective action of 3MA is associated with JNK inhibition

Finally, we explored if AMPK/mTORC1 axis, as the main intracellular energy balance-controlling signaling pathway, PI3K/Akt axis, which is known molecular target of 3MA, or cell survival/death-regulating MAPK members JNK and ERK, were involved in 3MA cytoprotective action. In accordance with the ability to cause energy depletion in B16 cells, 2DG/rotenone increased the phosphorylation (activation) of the energy sensor AMPK, while suppressing phosphorylation of the mTORC1 component mTOR and its target 4EBP1 (Fig. 6A). 3MA additionally activated AMPK and partly recovered the phosphorylation of mTOR and 4EBP1 (Fig. 6A). Despite increasing the toxicity of 2DG/rotenone, RNAi-mediated AMPK knockdown failed to exert a similar effect in 3MA-protected cells (Fig. 6B), thus arguing against the role of AMPK in the observed protection. Moreover, the activation of mTORC1 was not responsible for the cytoprotective effect of 3MA, as the latter was not affected by the mTORC1 inhibitor rapamycin (Fig. 6C). Expectedly, 3MA as a known PI3K inhibitor additionally potentiated 2DG/rotenone-mediated decrease in Akt phosphorylation (Fig. 6A). However, neither the pan-class I/II/III PI3K inhibitors wortmannin and LY29400 nor the Akt inhibitor DEBC were able to mimic the protective activity of 3MA (Fig. 6D), suggesting that it was independent of PI3K/Akt suppression. While upregulation of cAMP was responsible for some autophagy-independent biological effects of 3MA,[10,26] adenylate cyclase activator forskolin and cAMP agonist 8-Cl-cAMP did not reduce 2DG/rotenone cytotoxicity (Fig. 6E). 2DG to some extent increased and rotenone decreased the phosphorylation of the MAPK family member ERK, while the net ERK activation in the combination treatment was somewhat lower than that observed in untreated cells, and slightly increased by 3MA (Fig. 6A). ERK inhibitor PD98059 failed to affect the

Representative blots are shown, and densitometry data are presented as mean ± SD values of three independent experiments (B–D), or triplicates from representative of three independent experiments (A, E) (*$p < 0.05$, **$p < 0.01$, and ***$p < 0.001$ vs. no treatment; $^{\#\#}p < 0.01$ and $^{\#\#\#}p < 0.001$ vs. 2DG/rotenone (A), treatment with bafilomycin A1 alone (B), or cisplatin (D, E)).

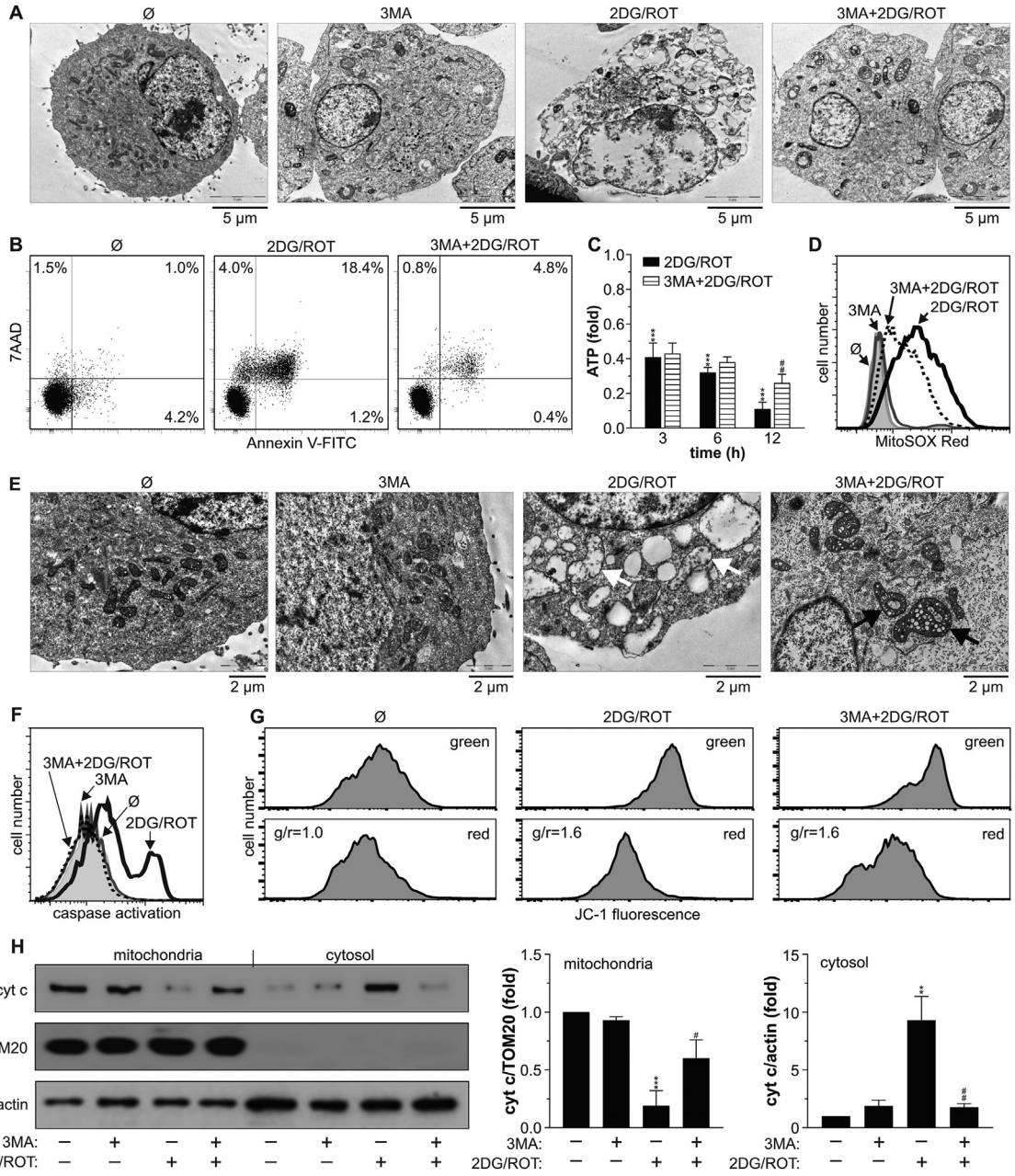

Fig. 5. 3MA-mediated protection from mitochondrial damage and necrotic death is associated with decrease in superoxide production. (A–H) B16 cells were incubated for 24 h (A), 12 h (B, D-H), or the indicated time periods (C) with 2DG (5 mM) or rotenone (ROT, 1 μM) alone and in combination, in the absence or presence of 3MA (5 mM). Cell ultrastructural morphology was analyzed by TEM (A, E), phosphatidylserine externalization (annexin$^+$ cells), cell membrane damage (7AAD$^+$ cells) (B), superoxide production (D), caspase activation (F), and mitochondrial membrane depolarization (G) were determined by flow cytometry, ATP concentration was measured by bioluminescence assay (C), and the levels of cytochrome *c* (cyt *c*) and TOM20 as a mitochondria-specific loading control in mitochondrial and actin in cytosol fractions were determined by immunoblot (H). Representative electron micrographs (A, E), flow cytometry dot-plots (B) or histograms (D, F, G) from one of two independent experiments with similar results are shown. The black and white arrows in (E) point to swollen but intact donut-shaped mitochondria and damaged mitochondria with fragmented cristae, respectively. Representative blots are shown, and densitometry data are presented as mean ± SD values of three independent experiments (H). The data in (C) are presented as mean ± SD values of triplicates from a representative of at least three experiments (**p < 0.01 and ***p < 0.01 vs. no treatment; $^{\#}$p < 0.01 and $^{\#\#}$p < 0.01 vs. treatment with 2DG/rotenone).

protective effect of 3MA (Fig. 6F), implying that protective activity of 3MA was independent of ERK. 2DG/rotenone combination caused a strong synergistic increase in the phosphorylation of another MAPK family member, JNK, which was markedly down-regulated by 3MA (Fig. 6A). JNK inhibitor SP600125 and JNK siRNA, which effectively reduced JNK phosphorylation and total levels (Fig. 6H and I), partly mimicked the protective action of 3MA (Fig. 6G, I) and mitigated mitochondrial damage (Fig. 6J) in 2DG/rotenone-treated cells. Therefore, the suppression of JNK, but not modulation of AMPK, mTORC1, PI3K/Akt, ERK, or cAMP, might participate in 3MA-mediated autophagy-independent protection from 2DG/rotenone cytotoxicity.

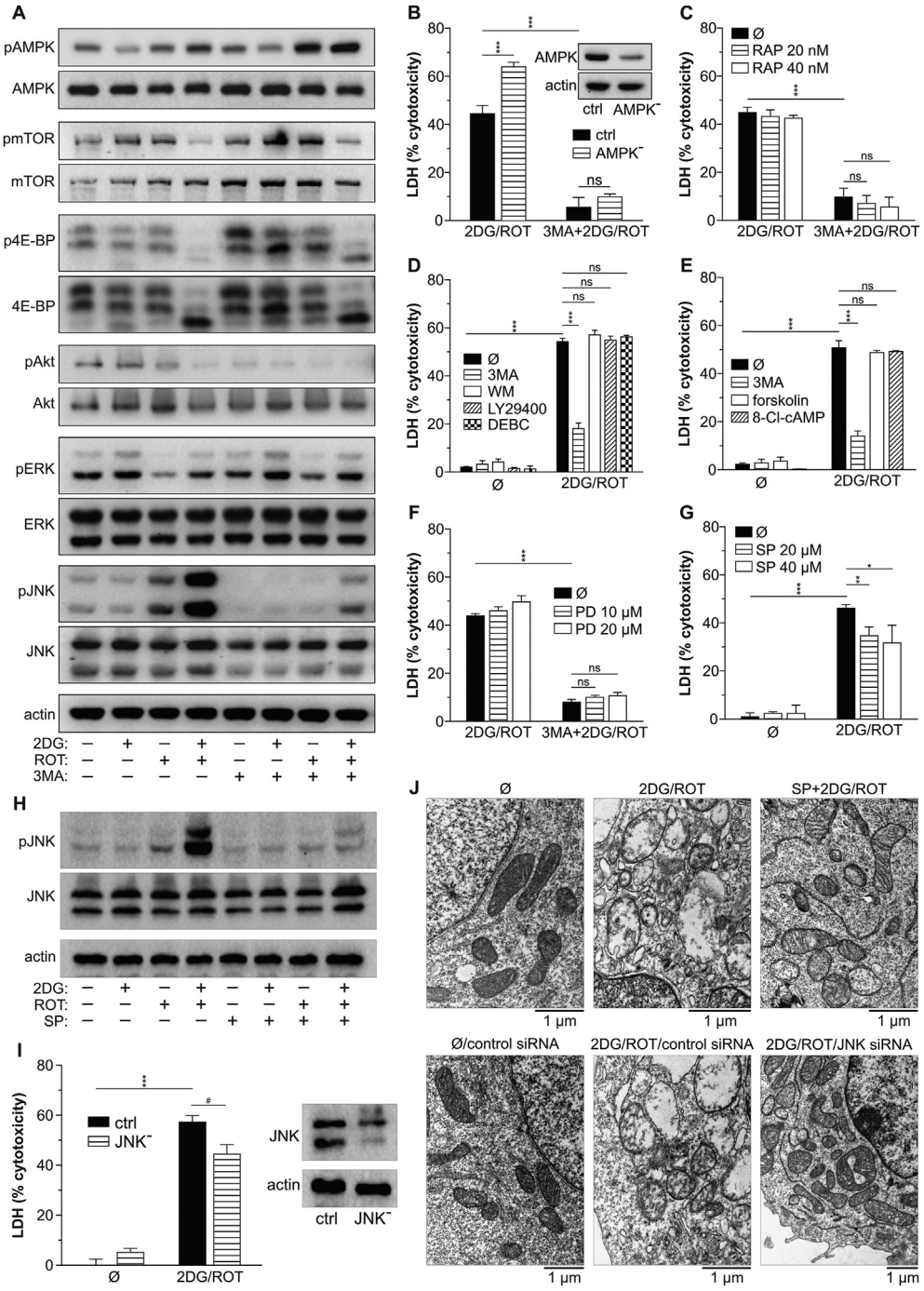

Fig. 6. Cytoprotective action of 3MA is associated with JNK inhibition. (A, C–H, J) B16 cells were incubated for 2 h (A, H), 24 h (C–G) or 12 h (J) with or without 2DG (5 mM)/rotenone (1 μM) in the absence or presence of 3MA (5 mM) (A, C, D, F), mTORC1 inhibitor rapamycin (10 nM) (C), PI3K inhibitors wortmannin (WM; 100 nM) and LY29400 (LY; 12.5 μM), Akt inhibitor DEBC (10 μM) (D), cAMP up-regulators forskolin (20 μM) and 8-Cl-cAMP (2 μM) (E), ERK inhibitor PD98059 (F), or JNK inhibitor SP600125 (G, H, J). (B, I, J) B16 cells transfected with control and AMPK siRNA (B) or JNK siRNA (I, J) were incubated with 2DG (5 mM)/rotenone (1 μM) in the absence or presence of 3MA (5 mM) (immunoblots confirm the efficiency of AMPK and JNK knockdown). The levels of phosphorylated/total AMPK, mTOR, 4E-BP1, Akt, ERK, and JNK were determined by immunoblot (A, H), cytotoxicity was measured by LDH test (B-G, I), while cell ultrastructural morphology was analyzed by TEM (J). Representative immunoblots from one of two independent experiments with similar results are shown (A, H). The data are presented as mean ± SD values of triplicates from a representative of at least three experiments (B-G, I) (*$p < 0.05$, **$p < 0.01$, and ***$p < 0.001$).

4. Discussion

We here demonstrate that a widely used autophagy inhibitor 3MA protects cancer cells from mitochondrial damage and necrosis induced by simultaneous blockade of glycolysis and oxidative phosphorylation. However, the observed protection was independent of autophagy modulation and possibly involved the suppression of JNK and decrease in mitochondrial superoxide production.

By using different cancer cell lines and experimental approaches, the present study confirms the concept that the fast metabolism and elevated energy demands make cancer cells more sensitive than

non-transformed cells to energy depletion induced by simultaneous targeting of glycolysis and oxidative phosphorylation.[27,28] More specifically, we have confirmed the previously reported ability of glycolysis inhibitor 2DG and mitochondrial complex I inhibitor rotenone to jointly induce cancer cells death.[29–31] Our data further expand on these studies by demonstrating that the ATP loss triggered by 2DG/rotenone is followed by a synergistic induction of superoxide production and mitochondrial swelling. Mitochondrial swelling is usually associated with the loss of mitochondrial membrane potential and opening of the MPT pore, a non-selective water- and solute-passing protein channel spanning the inner and outer mitochondrial membrane.[32] While confirming the role of oxidative stress, our data argue against the involvement of mitochondrial depolarization and MPT in 2DG/rotenone-induced mitochondrial damage. Namely, although mitochondrial complex I suppression by rotenone, in accordance with previous findings[33,34] readily triggered dissipation of mitochondrial membrane potential, the effect was counteracted by the known hyperpolarizing activity of 2DG.[35,36] Moreover, the MPT inhibitor cyclosporine A, in contrast to the antioxidant α-tocopherol, failed to reduce 2DG/rotenone-induced cytotoxicity in our experiments. Although somewhat unexpected, these findings agree with the studies demonstrating that mitochondrial swelling in some conditions could proceed without the involvement of mitochondrial depolarization and/or MPT.[32,37–39] However, while in these studies mitochondrial swelling led to the outer membrane rupture, release of cytochrome *c* from the intermembrane space and subsequent apoptosis, 2DG/rotenone treatment in our experiments caused necrotic cell demise insensitive to the inhibition of programmed cell death (apoptosis and necroptosis). Despite mitochondrial release of cytochrome *c* and caspase activation, we did not demonstrate any PARP activation, DNA fragmentation, and apoptotic death in 2DG/rotenone-treated cells. This is consistent with the fact that the nuclear translocation of active caspases and DNA degradation require ATP.[40,41] Accordingly, ATP depletion readily converts apoptosis to necrosis.[40,42] In agreement with the ability of the pro-death kinase JNK to participate in mitochondrial damage and necrosis induced by various cytotoxic stimuli, including energy deprivation,[43,44] our data indicate the possible role of JNK in 2DG/rotenone-mediated mitochondrial dysfunction and necrosis.

In accordance with the proposed mechanisms of 2DG/rotenone cytotoxicity, the ability of 3MA to prevent 2DG/rotenone-triggered necrosis was associated with the partial ATP recovery and decrease in mitochondrial swelling, superoxide production, and JNK activation. However, the 3MA-mediated restoration of ATP levels did not occur before 12 h of treatment and was rather moderate, indicating that it was probably a consequence, rather than a cause of improved mitochondrial function. Interestingly, 3MA treatment and JNK suppression in our experiments increased the presence of donut-shaped (toroidal) mitochondria, which are produced by anomalous fusion events and tolerate matrix volume increases more effectively, giving rise to offspring that can regain normal function.[45] Moreover, antioxidant treatment and JNK suppression, partly but less effectively than 3MA, protected 2DG/rotenone-exposed cells, indicating a possible partial relevance of these events in the pro-survival action of 3MA. Having in mind a complex feedback network between mitochondrial superoxide production, JNK activation, and cytochrome *c* release, one could assume that the latter could also contribute to 3MA-mediated protection. Namely, mitochondrial superoxide generation and JNK stimulate each other,[46] while both increase the permeability of outer mitochondrial membrane and subsequent cytochrome *c* release.[47,48] In turn, a decrease in mitochondrial levels of cytochrome *c*, which in its oxidized state acts as a superoxide scavenger, could further promote ROS accumulation,[49] thus potentially increasing mitochondrial damage and cell demise independently of its role in caspase-mediated apoptosis. Indeed, some data indicate that cytochrome *c* release from mitochondria might regulate not only apoptotic, but also some forms of necrotic cell death.[50,51] It remains on further studies to explore the role of superoxide-JNK interplay and cytochrome *c* in 3MA pro-survival action in energy stress caused by 2DG/rotenone combination. Moreover, although 3MA has been reported to affect various signaling pathways,[8,10,13] our data obtained with appropriate pharmacological modulators argue against the involvement of AMPK, mTORC1, PI3K/Akt, ERK, or cAMP in its protective effect against 2DG/rotenone-triggered necrosis.

Our results are consistent with the ability of 3MA to inhibit mitochondrial swelling and cytochrome *c* release in neurons exposed to calcium or phenylarsine oxide,[12] as well as JNK activation in nerve growth factor-deprived neurons.[13] However, while these studies did not directly examine the role of autophagy modulation in the cytoprotective actions of 3MA, we clearly demonstrate that neither inhibition nor induction of autophagy by 3MA was involved in the protection from 2DG/rotenone-triggered cytotoxicity. Namely, lysosome inhibitors (bafilomycin A1, chloroquine, NH_4Cl) and PI3K-blocking autophagy modulators (wortmannin, LY29400), as well as RNAi knockdown of beclin-1 or LC3, all failed to mimic 3MA-mediated cytoprotection. The decrease of autophagic flux by 2DG/rotenone and inability of 3MA to further affect it supports our conclusion that the pro-survival action of 3MA was independent of autophagy inhibition. This might seem surprising, having in mind that autophagy is usually activated in conditions of limiting energy supply, as well as that AMPK/mTORC1 energy-sensing signaling axis was readily engaged by 2DG/rotenone treatment in our experiments. On the other hand, autophagy itself requires ATP, especially for the initiation steps.[52] It is therefore plausible to assume that the ATP levels in 2DG/rotenone-exposed cells may have fell below the minimal energetic threshold necessary for an adequate autophagic response. Indeed, autophagy was reduced in cancer cells treated with 2DG in combination with the mitochondrial ATP synthase inhibitor oligomycin,[53] mitochondrial complex I inhibitor metformin,[54] or moderate hypoxia.[55] This correlated with dramatic depletion of ATP, transcriptional downregulation of autophagy, and decreased levels of ATG5/ATG12 and PI3K class III/beclin-1 complexes.[55] Accordingly, we have observed a reduction in beclin-1 levels in 2DG/rotenone-treated cells, which further confirms the inhibition of autophagy in our experimental model of intracellular energy depletion. Finally, the inability of beclin-1 or LC3 knockdown to reduce the protective effect of 3MA confirmed that it was not mediated by its previously reported ability to induce autophagy through PI3K class I/mTOR suppression.[8]

In conclusion, the results of the present study warrant caution when attributing the cytoprotective effects of 3MA to autophagy inhibition without the additional proof. They also indicate that autophagy suppression might not be effective, and 3MA could be even detrimental, in therapeutic killing of cancer cells in which autophagy is already suppressed by a severe energy deficit. Finally, in light of the findings showing measurable levels of endogenous 3MA in chemotherapy-receiving patients, it would be interesting to explore if the release of 3MA from mutated DNA might serve as a survival mechanism for energy-stressed or drug-treated tumor cells.

Declaration of competing interest

The authors declare no conflict of interest.

Author contributions

Milica Kosic: Investigation. Verica Paunovic: Conceptualization, Investigation, Writing - Reviewing and Editing. Biljana Ristic: Investigation. Aleksandar Mircic: Investigation. Mihajlo Bosnjak:

Investigation. Danijela Stevanovic: Investigation. Tamara Kravic-Stevovic: Writing - Reviewing and Editing. Vladimir Trajkovic: Conceptualization, Writing - Reviewing and Editing, Project administration. Ljubica Harhaji-Trajkovic: Conceptualization, Validation, Formal analysis, Writing - Original Draft, Visualization, Supervision.

Acknowledgements

This study was supported by the Ministry of Education, Science and Technological Development of the Republic of Serbia, Contract No. 451-03-9/2021-14/200007 and 451-03-9/2021-14/200110. Verica Paunovic is a recipient of the UNESCO L'OREAL national scholarship program "For Women in Science" (contract number 403F). The authors thank Dr. Ljubica Vucicevic and Dr. Maja Misirkic-Marjanovic (Department of Neurophysiology, Institute for Biological Research, "Sinisa Stankovic"- National Institute of Republic of Serbia, University of Belgrade) for technical assistance with immunoblotting, Dr. Nina Krako Jakovljevic (Clinic for Endocrinology, Diabetes and Metabolic Diseases, Clinical Centre of Serbia) for providing CCCP, and Dragan Besevic and Milos Kis (Institute of Histology and Embryology, Faculty of Medicine, University of Belgrade) for technical assistance in TEM.

References

1. Dikic I, Elazar Z. Mechanism and medical implications of mammalian autophagy. *Nat Rev Mol Cell Biol*. 2018;19(6):349–364.
2. Maiuri MC, Kroemer G. Therapeutic modulation of autophagy: which disease comes first? *Cell Death Differ*. 2019;26(4):680–689.
3. Linder B, Kögel D. Autophagy in cancer cell death. *Biology*. 2019;8(4).
4. Pasquier B. Autophagy inhibitors. *Cell Mol Life Sci*. 2016;73(5):985–1001.
5. Tseng HC, Liu WS, Tyan YS, Chiang HC, Kuo WH, Chou FP. Sensitizing effect of 3-methyladenine on radiation-induced cytotoxicity in radio-resistant HepG2 cells in vitro and in tumor xenografts. *Chem Biol Interact*. 2011;192(3):201–208.
6. Zhao X, Gao S, Ren H, Huang H, Ji W, Hao J. Inhibition of autophagy strengthens celastrol-induced apoptosis in human pancreatic cancer in vitro and in vivo models. *Curr Mol Med*. 2014;14(4):555–563.
7. Liu Z, He K, Ma Q, et al. Autophagy inhibitor facilitates gefitinib sensitivity in vitro and in vivo by activating mitochondrial apoptosis in triple negative breast cancer. *PloS One*. 2017;12(5), e0177694.
8. Wu YT, Tan HL, Shui G, et al. Dual role of 3-methyladenine in modulation of autophagy via different temporal patterns of inhibition on class I and III phosphoinositide 3-kinase. *J Biol Chem*. 2010;285(14):10850–10861.
9. Wang S, Li J, Du Y, et al. The Class I PI3K inhibitor S14161 induces autophagy in malignant blood cells by modulating the Beclin 1/Vps34 complex. *J Pharmacol Sci*. 2017;134(4):197–202.
10. Caro LH, Plomp PJ, Wolvetang EJ, Kerkhof C, Meijer AJ. 3-Methyladenine, an inhibitor of autophagy, has multiple effects on metabolism. *Eur J Biochem*. 1988;175(2):325–329.
11. Mizushima N, Yamamoto A, Hatano M, et al. Dissection of autophagosome formation using Apg5-deficient mouse embryonic stem cells. *J Cell Biol*. 2001;152(4):657–668.
12. Xue L, Borutaite V, Tolkovsky AM. Inhibition of mitochondrial permeability transition and release of cytochrome c by anti-apoptotic nucleoside analogues. *Biochem Pharmacol*. 2002;64(3):441–449.
13. Xue L, Fletcher GC, Tolkovsky AM. Autophagy is activated by apoptotic signalling in sympathetic neurons: an alternative mechanism of death execution. *Mol Cell Neurosci*. 1999;14(3):180–198.
14. Cheng SY, Chen NF, Kuo HM, et al. Prodigiosin stimulates endoplasmic reticulum stress and induces autophagic cell death in glioblastoma cells. *Apoptosis*. 2018;23(5–6):314–328.
15. Liu H, Wang L, Zeng Q, et al. Oxidative stress-mediated autophagic cell death participates in the neurotoxic effect on SH-SY5Y cells induced by excessive iodide. *Environ Toxicol*. 2018;33(8):851–860.
16. Zhang M, Kim HS, Jin T, Moon WK. Near-infrared photothermal therapy using EGFR-targeted gold nanoparticles increases autophagic cell death in breast cancer. *J Photochem Photobiol, B*. 2017;170:58–64.
17. Wyatt MD, Allan JM, Lau AY, Ellenberger TE, Samson LD. 3-methyladenine DNA glycosylases: structure, function, and biological importance. *Bioessays*. 1999;21(8):668–676.
18. Braybrooke JP, Houlbrook S, Crawley JE, et al. Evaluation of the alkaline comet assay and urinary 3-methyladenine excretion for monitoring DNA damage in melanoma patients treated with dacarbazine and tamoxifen. *Canc Chemother Pharmacol*. 2000;45(2):111–119.
19. Bobola MS, Kolstoe DD, Blank A, Chamberlain MC, Silber JR. Repair of 3-methyladenine and abasic sites by base excision repair mediates glioblastoma resistance to temozolomide. *Front Oncol*. 2012;2:176.
20. Kosic M, Arsikin-Csordas K, Paunovic V, et al. Synergistic anticancer action of lysosomal membrane permeabilization and glycolysis inhibition. *J Biol Chem*. 2016;291(44):22936–22948.
21. Chow CK. Vitamin E regulation of mitochondrial superoxide generation. *Biol Signals Recept*. 2001;10(1–2):112–124.
22. Tanida I, Minematsu-Ikeguchi N, Ueno T, Kominami E. Lysosomal turnover, but not a cellular level, of endogenous LC3 is a marker for autophagy. *Autophagy*. 2005;1(2):84–91.
23. Harhaji-Trajkovic L, Vilimanovich U, Kravic-Stevovic T, Bumbasirevic V, Trajkovic V. AMPK-mediated autophagy inhibits apoptosis in cisplatin-treated tumour cells. *J Cell Mol Med*. 2009;13(9B):3644–3654.
24. Ahmad T, Aggarwal K, Pattnaik B, et al. Computational classification of mitochondrial shapes reflects stress and redox state. *Cell Death Dis*. 2013;4(1):e461.
25. Bernardi P, Scorrano L, Colonna R, Petronilli V, Di Lisa F. Mitochondria and cell death. Mechanistic aspects and methodological issues. *Eur J Biochem*. 1999;264(3):687–701.
26. Heckmann BL, Yang X, Zhang X, Liu J. The autophagic inhibitor 3-methyladenine potently stimulates PKA-dependent lipolysis in adipocytes. *Br J Pharmacol*. 2013;168(1):163–171.
27. Gogvadze V, Zhivotovsky B, Orrenius S. The Warburg effect and mitochondrial stability in cancer cells. *Mol Aspect Med*. 2010;31(1):60–74.
28. Lee M, Yoon JH. Metabolic interplay between glycolysis and mitochondrial oxidation: the reverse Warburg effect and its therapeutic implication. *World J Biol Chem*. 2015;6(3):148–161.
29. Dier U, Shin DH, Hemachandra LP, Uusitalo LM, Hempel N. Bioenergetic analysis of ovarian cancer cell lines: profiling of histological subtypes and identification of a mitochondria-defective cell line. *PloS One*. 2014;9(5), e98479.
30. Fath MA, Diers AR, Aykin-Burns N, Simons AL, Hua L, Spitz DR. Mitochondrial electron transport chain blockers enhance 2-deoxy-D-glucose induced oxidative stress and cell killing in human colon carcinoma cells. *Cancer Biol Ther*. 2009;8(13):1228–1236.
31. Liu H, Hu YP, Savaraj N, Priebe W, Lampidis TJ. Hypersensitization of tumor cells to glycolytic inhibitors. *Biochemistry*. 2001;40(18):5542–5547.
32. Halestrap AP. Calcium, mitochondria and reperfusion injury: a pore way to die. *Biochem Soc Trans*. 2006;34(Pt 2):232–237.
33. Fortalezas S, Marques-da-Silva D, Gutierrez-Merino C. Creatine protects against cytosolic calcium dysregulation, mitochondrial depolarization and increase of reactive oxygen species production in rotenone-induced cell death of cerebellar granule neurons. *Neurotox Res*. 2018;34(3):717–732.
34. Moon Y, Lee KH, Park JH, Geum D, Kim K. Mitochondrial membrane depolarization and the selective death of dopaminergic neurons by rotenone: protective effect of coenzyme Q10. *J Neurochem*. 2005;93(5):1199–1208.
35. Giammarioli AM, Gambardella L, Barbati C, et al. Differential effects of the glycolysis inhibitor 2-deoxy-D-glucose on the activity of pro-apoptotic agents in metastatic melanoma cells, and induction of a cytoprotective autophagic response. *Int J Cancer*. 2012;131(4):E337–E347.
36. Wojtczak L, Teplova VV, Bogucka K, et al. Effect of glucose and deoxyglucose on the redistribution of calcium in ehrlich ascites tumour and Zajdela hepatoma cells and its consequences for mitochondrial energetics. Further arguments for the role of Ca(2+) in the mechanism of the crabtree effect. *Eur J Biochem*. 1999;263(2):495–501.
37. Eliseev RA, Gunter KK, Gunter TE. Bcl-2 sensitive mitochondrial potassium accumulation and swelling in apoptosis. *Mitochondrion*. 2002;1(4):361–370.
38. Galindo MF, Jordan J, Gonzalez-Garcia C, Cena V. Reactive oxygen species induce swelling and cytochrome c release but not transmembrane depolarization in isolated rat brain mitochondria. *Br J Pharmacol*. 2003;139(4):797–804.
39. Gogvadze V, Robertson JD, Enoksson M, Zhivotovsky B, Orrenius S. Mitochondrial cytochrome c release may occur by volume-dependent mechanisms not involving permeability transition. *Biochem J*. 2004;378(Pt 1):213–217.
40. Leist M, Single B, Castoldi AF, Kuhnle S, Nicotera P. Intracellular adenosine triphosphate (ATP) concentration: a switch in the decision between apoptosis and necrosis. *J Exp Med*. 1997;185(8):1481–1486.
41. Yasuhara N, Eguchi Y, Tachibana T, Imamoto N, Yoneda Y, Tsujimoto Y. Essential role of active nuclear transport in apoptosis. *Gene Cell : Devoted Mol Cell Mech*. 1997;2(1):55–64.
42. Eguchi Y, Shimizu S, Tsujimoto Y. Intracellular ATP levels determine cell death fate by apoptosis or necrosis. *Cancer Res*. 1997;57(10):1835–1840.
43. Song X, Li T. Ripk3 mediates cardiomyocyte necrosis through targeting mitochondria and the JNK-Bnip3 pathway under hypoxia-reoxygenation injury. *J Recept Signal Transduct Res*. 2019;39(4):331–340.
44. Yaglom JA, Ekhterae D, Gabai VL, Sherman MY. Regulation of necrosis of H9c2 myogenic cells upon transient energy deprivation. Rapid deenergization of mitochondria precedes necrosis and is controlled by reactive oxygen species, stress kinase JNK, HSP72 and ARC. *J Biol Chem*. 2003;278(50):50483–50496.
45. Liu X, Hajnoczky G. Altered fusion dynamics underlie unique morphological changes in mitochondria during hypoxia-reoxygenation stress. *Cell Death Differ*. 2011;18(10):1561–1572.
46. Chambers JW, LoGrasso PV. Mitochondrial c-Jun N-terminal kinase (JNK) signaling initiates physiological changes resulting in amplification of reactive oxygen species generation. *J Biol Chem*. 2011;286(18):16052–16062.

47. Madesh M, Hajnoczky G. VDAC-dependent permeabilization of the outer mitochondrial membrane by superoxide induces rapid and massive cytochrome c release. *J Cell Biol*. 2001;155(6):1003–1015.
48. Tournier C, Hess P, Yang DD, et al. Requirement of JNK for stress-induced activation of the cytochrome c-mediated death pathway. *Science*. 2000;288(5467):870–874.
49. Pasdois P, Parker JE, Griffiths EJ, Halestrap AP. The role of oxidized cytochrome c in regulating mitochondrial reactive oxygen species production and its perturbation in ischaemia. *Biochem J*. 2011;436(2):493–505.
50. Atlante A, Calissano P, Bobba A, Azzariti A, Marra E, Passarella S. Cytochrome c is released from mitochondria in a reactive oxygen species (ROS)-dependent fashion and can operate as a ROS scavenger and as a respiratory substrate in cerebellar neurons undergoing excitotoxic death. *J Biol Chem*. 2000;275(47):37159–37166.
51. Chen SP, Wu JL, Su YC, Hong JR. Anti-Bcl-2 family members, zfBcl-x(L) and zfMcl-1a, prevent cytochrome c release from cells undergoing betanodavirus-induced secondary necrotic cell death. *Apoptosis: Int J Program cell Death*. 2007;12(6):1043–1060.
52. Loos B, Engelbrecht AM, Lockshin RA, Klionsky DJ, Zakeri Z. The variability of autophagy and cell death susceptibility: unanswered questions. *Autophagy*. 2013;9(9):1270–1285.
53. Xi H, Kurtoglu M, Liu H, et al. 2-Deoxy-D-glucose activates autophagy via endoplasmic reticulum stress rather than ATP depletion. *Canc Chemother Pharmacol*. 2011;67(4):899–910.
54. Ben Sahra I, Laurent K, Giuliano S, et al. Targeting cancer cell metabolism: the combination of metformin and 2-deoxyglucose induces p53-dependent apoptosis in prostate cancer cells. *Cancer Res*. 2010;70(6):2465–2475.
55. Xi H, Barredo JC, Merchan JR, Lampidis TJ. Endoplasmic reticulum stress induced by 2-deoxyglucose but not glucose starvation activates AMPK through CaMKKbeta leading to autophagy. *Biochem Pharmacol*. 2013;85(10):1463–1477.